Supplementary Information

A Methods

A.1 Culturing hippocampal neurons on patterned coverslips.

Primary cultures were prepared as described in Papa et al.[1]. In brief, 19-day-old embryos were taken from Wistar rats, the brains removed and the hippocampi dissected out and dissociated by mechanical trituration. Cells were plated in *1ml* plating medium (Eagle's MEM supplemented by *5%* heat inactivated horse serum, *5%* heat inactivated fetal calf serum, *0.6%* glucose, gentamicin (*20μg/ml*), glutamax (Gibco), and B27 supplement (*1μl/ml*)) onto the previously patterned coverslips (see Coverslip patterning in the Methods section) at *330,000* cells per dish. The cells were incubated at *37°C*, *5%* CO_2 in plating medium. After 3 days the medium was replaced, with no fetal calf serum, *10%* heat inactivated horse serum and *0.2mg/ml* 5-Fluoro-2′-deoxyuridine (FUDR, Sigma-Aldrich) and *0.5mg/ml* Uridine (Sigma-Aldrich) added to inhibit further division of the glial cells. Fluids are exchanged again 3 days later (day 6 in culture) to the final medium, which includes *10%* heat inactivated horse serum, glucose, gentamicin and glutamax (concentrations as above).

Neurons and glial cells initially settled down over the complete coverslip. The cells that landed on the patterned locations adhered and started growing in a matter of hours. The rest of the cells either connected to cells on the patterns and were pulled towards them or died and were washed away. The glia serve as a support layer for the neurons, and are also able to grow only on the patterns. Axonal growth cones developed from as early as one hour after plating and a densely connected network was observed as early as day 3 in culture. The cultures were measured (see A.2) between day 14 and 21 in culture but these cultures keep their global patterned structure and remain functional for as long as 2 months. A previous report describes one-dimensional cultures in more details[2].

While other protocols have shown that cells can grow on *50μm* wide lines, in our experiments they do not. We can think of two reasons for this difference: first, the adhesives used in our protocol (Laminin and Fibronectin) are weaker than those commonly used (PLL, PEI, MatriGel). We use weak adhesives specifically to assure that any leakage of these proteins outside the patterned regions will be insufficient for neurons to grow on. Second, thin lines are patterned adjacent to neighboring thicker lines, so that cells growing on the thicker lines adhere better to the surface and can pull cells growing on the thin section to migrate towards them. These are very interesting motile processes that have often been observed in our lab, in which axonal bundles exert forces on the cells, with a subsequent motion towards each other if they are not well anchored. The improved adhesion to the thick lines ensures that cells growing there will usually win this 'tug of war'. If the thin line is very long then some aggregates can survive, a fact that puts some constraints on the length of the thin line in the Threshold device.

A.2 Imaging neuronal activity with calcium-sensitive fluorescent dyes.

Cells were measured between day 14 and 21 in culture. Prior to measurement, cells were incubated for *60min* with *2μg/ml* of the calcium-sensitive, cell-permeant dye Fluo4-AM (Invitrogen), in a recording solution that consists of *128mM* NaCl, *4mM* KCl, *1mM* CaCl2, *1mM* MgCl2, *45mM* sucrose, *10mM* glucose, and *0.01M* HEPES with the pH titrated to *7.4*. Cells were then placed in fresh recording solution. The culture was imaged with a Zeiss Axiovert 135TV inverted microscope, photographed through a *5X* or *10X* lens by a Hamamatsu C2400-87 CCD camera fitted with a *0.5X* adapter to enlarge the field of view. Epi-fluorescence images of activity using an XF100-2 filter set (Omega

Optical) were captured at *25Hz*, stored on videotape, and digitized with a PCI-1411 frame grabber (National Instruments) using a specially designed software (based on Labview and IMAQ, National Instruments). De-interlacing prior to the subsequent off-line analysis increased the time resolution to *50Hz*.

A.3 Green Fluorescent Protein (GFP) Transfections.

To visualize neuronal processes, cells were transfected one day after plating using the pEF/myc/cyto/GFP plasmid containing nonspecific GFP (Invitrogen). During transfection the plating medium was replaced with warm *500μl* optiMEM1 (Invitrogen). Cells were left to incubate for *20min* while the DNA was prepared. *2.5μl* of Lipofectamin2000 (Invitrogen) were diluted in *100μl* of optiMEM1 (Gibco). After *5min*, *1.25μg* of the plasmid were added and after an additional *20min* the solution was added to the culture. After *40min* of incubation the DNA solution was replaced with the original plating medium. Epi-fluorescence imaging was performed *8-11* days after plating, with a Zeiss Axiovert 135TV inverted microscope, photographed through a *10X* or *40X* lens. The number of processes was counted either directly under the microscope or from stored high resolution (*2560x1920* pixels) images of the same field of view, with similar results.

Transfection efficiency was measured to be one transfected cell in approximately 100 cells (See Sections B.1 and B.3).

A.4 Data Analysis.

Analysis of calcium transients into population spikes was done as reported previously[2]. Relative timing of bursts was determined by comparing the frames at which the calcium level reached its half peak value. Images with GFP were analyzed using ImageJ software[3]. To analyze images, we first used an alignment toolbox[4] to align consecutive images and then utilized a tracking toolbox to manually track processes that were observed in the frame. The recorded coordinates were further analyzed using Matlab (Mathworks) to extract statistical measures regarding the length and direction of these segments (see SI for details). To fit the data we performed a Non-Linear Least Square fit using the "Trust-Region" algorithm with Matlab Curve Fitting Toolbox. Error estimates given for fitted values are the *95%* confidence limits, while for the measured data they are the Standard Error of the Mean.

B Counting the number of neurons that send axons across a barrier

Using the GFP images, we measure the average number of stained axonal branches A that cross the barrier. We can identify the stained cells of origin for most of these branches, and measure the average number of axonal branches Ψ that a stained cell sends across the barrier. Thus the average number of GFP stained cells that send axons across a barrier is equal to A/Ψ. To obtain the total number M of cells (stained and non-stained) that send axons across the barrier we multiply it by the staining efficiency e_{GFP} of the GFP transfection, $M=A/\Psi/e_{GFP}$.

To obtain the staining efficiency we measure the average total number of cells (stained and non-stained) C_T in the device and the number of observed stained cells C_S. We then obtain e_{GFP} By dividing C_S by C_T, $e_{GFP}=C_S/C_T$. The efficiency is measured for the different devices separately, but the numbers are found to be very similar.

All measurements are given by their mean and its standard error unless mentioned otherwise.

B.1 Threshold component.

The average number of axonal branches crossing in *9* Threshold barriers was: $A_{thr}=3.2\pm0.4$. By identifying the cells of origin in *7* of these Threshold devices we found that the average number of branches that one cell sends across the barrier was $\Psi_{thr}=1.6\pm0.3$. The average number of stained cells found on one side of the Threshold device (thick line) was $C_S=3.1\pm0.4$, while the average number of neurons constituting each thick line was $C_T=347\pm22$, so that $1/e_{GFP}=112\pm17$ (one GFP stained cell for every *112* cells).

From these measurements we calculate $2M_{thr}=A_{thr}/\Psi_{thr}/e_{GFP}=231\pm68$ cells. The number of cells crossing in one direction is on average half of that: $M_{thr}=116\pm34$ cells.

B.2 AND Gate.

The AND Gate is comprised of two parallel Threshold devices, and we therefore take the number of cells crossing from both the Input regions to the Output region to be twice that of the Threshold: $M_{AND}=231\pm68$ cells.

B.3 Neuronal Diode.

The average number of axonal branches crossing the barrier between *9* pairs of triangles in a neuronal Diode was: $A_{Diode}=8.6\pm1.2$. By identifying the cells of origin (blue and red circles in Figure S1a) of *56* out of a total of *78* axons we found that the average number of branches that one cell sends across the barrier was $\Psi_{Diode}=2.0\pm0.3$. The average number of stained cells on one triangle was $C_S=3.5\pm0.7$ while the average number of neurons found on each triangle was $C_T=384\pm25$, so that $1/e_{GFP}=111\pm23$ (one GFP stained cell for every *111* cells, in good agreement with the measurement from the Threshold device).

From these measurements we calculate $M_{Diode}=A_{Diode}/\Psi_{Diode}/e_{GFP}=484\pm121$ cells.

The ratio $\Gamma\approx M_{fwd}/M_{bwd}$ between the number of forward and backward crossings in the Diode was measured in the *9* crossings. The highest ratio was $\Gamma\approx3$, measured in 2 of the diodes, and the lowest was $\Gamma\approx½$ measured in another 2 of the diodes. On average the ratio was $\Gamma\approx1.3\pm0.3$. This explains the fact that only around 20% of the Diodes function well while the rest function as transmission lines. When simulating axonal growth in a triangle (see section C.3) we get a ratio of $\Gamma\approx3.1$. The ratio chosen for the model was $\Gamma\approx3$ since we describe those diodes that function well, and only data from their activity was used for analysis. The number of cells crossing between triangles is therefore distributed as follows:

$M_{fwd}+M_{bwd}=484\pm121$ cells.

$M_{fwd}/M_{bwd}=3$.

$M_{fwd}=363\pm115$ cells crossing forward.

$M_{bwd}=121\pm39$ cells crossing backward.

C Analyzing and simulating axonal trajectories in the Diode

Analysis of the GFP images of neuronal Diodes reveals two rules that dominate the growth: axons don't grow outside the patterned areas, and they tend to minimize the amount and magnitude of their turns. We quantify these rules in section C.1 and then use them to simulate axonal growth in the Diode in section C.2. To validate our simulation we show that it can reconstruct the measured axonal orientation histograms. Finally, we

use the simulation to obtain the number of cells that send axons forward compared to those that send axons backwards across the Diode (section C.3).

C.1 Measurements of axonal configurations

Quantitative analysis of the GFP images was performed manually (using ImageJ software[3]) as follows: axons were identified as long and uniformly thin processes, while dendrites were identified as processes with diameters that become thinner distal from the soma and branch extensively at angles that are much smaller than $90°$.

Axons were followed in two different ways. In the first technique *1263* partial segments of axons were identified and tracked in the GFP images of 11 triangles (see Figure S1a). The segments were considered undirected, i.e. symmetric with respect to a rotation by an angle π. In the second technique we tracked the full trajectory of *44* axonal branches, from their cell of origin to their end.

From the axonal segments we obtained the following information:

1. Directional histograms of segmental orientation at locations in the triangle that coincide with the lattice of the simulations described in section C.2. The histogram at each location integrates information from all segments that pass by that location (Figure 3d in the manuscript).

From the complete axonal branches we obtained the following information:

2. The distribution of total axonal lengths is shown in Figure S1c. The average length of these axons was $800\mu m$.
3. The persistence length L of axons, calculated as the exponential decay length of the cosine of the angular difference ϕ between axonal segments that are a distance x apart: $\langle \cos\phi \rangle = e^{-x/L}$. This yielded a value of $L=420\pm50\mu m$.
4. The histogram of angles between adjacent axonal steps taken at the size of the simulation lattice (see below and Figure 3c in the manuscript).

A consistency check was performed by comparing the persistence length and the histogram of angles obtained either from the axonal segments or from the complete branches. Similar values were obtained in both methods, well within the experimental error.

C.2 Simulations of the directional histogram of axonal segments

We simulated axonal growth in the Diode using a hexagonal lattice with G points. The spacing a between nearest neighbors was chosen as the width of the region that connects between the two triangles $a=50\mu m$. Axonal propagation on the lattice was determined by the following rules:

1. Only transitions between nearest neighbors were allowed.
2. The probability of an axon to change its direction at each step was calculated using the histogram of angles.
3. Transitions outside the borders of the triangle were not allowed. Periodic boundary conditions at the apex of the triangle and the center of its base enabled the simulation of axons that cross from one triangle to another.
4. The number of axons was conserved.

The simulation operates on an 'occupation' matrix s of size $Gx6$ whose (i,j)'th element specifies the number of axonal edges, or 'growth cones', that are expected to be found entering site i from direction j. A probability transition operator T_{ijkl} is then defined,

comprising of the probabilities for a transition from state *(i,j)* to state (*k,l*). This is the probability for an axon that entered site *i* at an angle *j* to enter site *k* at an angle *l*, and is set by the axonal propagation rules above. The angular transition probabilities in *T* were symmetric with respect to right or left turns (but not front or back!), leaving four independent angular transition probabilities.

The simulation begins by specifying an initial occupation matrix s^o. Applying the transition operator *n* times on the initial occupation matrix results in a new matrix s^n, whose coordinates represent the number of growth cones of axons with length $n \cdot a$ that are expected to be found at any location and direction.

We used an initial matrix s_o that contained six axonal growth cones at every location where a cell soma was observed in any of the measured GFP images (circles in Figure S1a). The axonal growth cones were initially evenly distributed in all six directions of the lattice. The simulation was run until the simulated axons reached a length of $800\mu m$. At each simulation step the number and direction of growth cones that were present at each location was stored.

The directional histogram was calculated by summing over the number of axons pointing at each direction in every location on the lattice. We verified that the simulation produces quantitatively similar axonal configurations as the Diode, comparing it to the measured one (Figure 3d in the manuscript). Since the allowed directions of the growth cone on the lattice were six, the experimental histogram of angles was regrouped in six bins.

The simulated and measured histograms provide two series of Nx6 probabilities, with indices of position and direction respectively. The absolute value of the difference between the two series, averaged over all points and over all directions, is *40%*. The correlation between the two series of points is $R=0.6$.

The major advantage of this simulation is that local information, i.e. the directional histogram at every point, was obtained from global information such as the averaged angle histogram and the geometry of the pattern boundaries.

C.3 Simulations of the number of cells that send axons forward and backward across the Diode barrier.

To estimate the ratio between the numbers of cells sending axons forward to the next triangle versus those sending axons backwards to the previous one we used a simulation based on the one described above, with the following changes:

1. Local information was added by considering the directional histogram at every point. The probability of an axon to change its direction at each step (rule #2 of the simulation described above) was different for each location on the lattice. This probability was calculated by multiplying the histogram of angles (used in rule #2 above) by the experimentally measured directional histogram of this location, and renormalizing to conserve the number of axons. This modification relies on the experimental observation that axons tend to propagate in parallel to other axons along existing pathways.
2. The periodic boundary conditions were cancelled to prevent long axons from crossing between triangles more than once. Instead, two perfect sinks were imposed by the transition matrix one at the apex and another at the center of the triangle base. These sinks were used to accumulate the number of axons that crossed between triangles in the simulation.
3. We used an initial matrix so that contained 384 growth cones (corresponding to the average measured number of cells in one triangle) uniformly distributed among the locations and directions of the whole lattice.

4. The dependence on axon length was investigated by letting the simulation run until the simulated axons reached a length of 3000μm. At each simulation step the numbers of growth cones that crossed forward or backward and accumulated in the sinks (see above) were stored. The ratio Γ of cumulative forward to cumulative backward crossings as a function of the length is plotted in Figure S1c (red line).

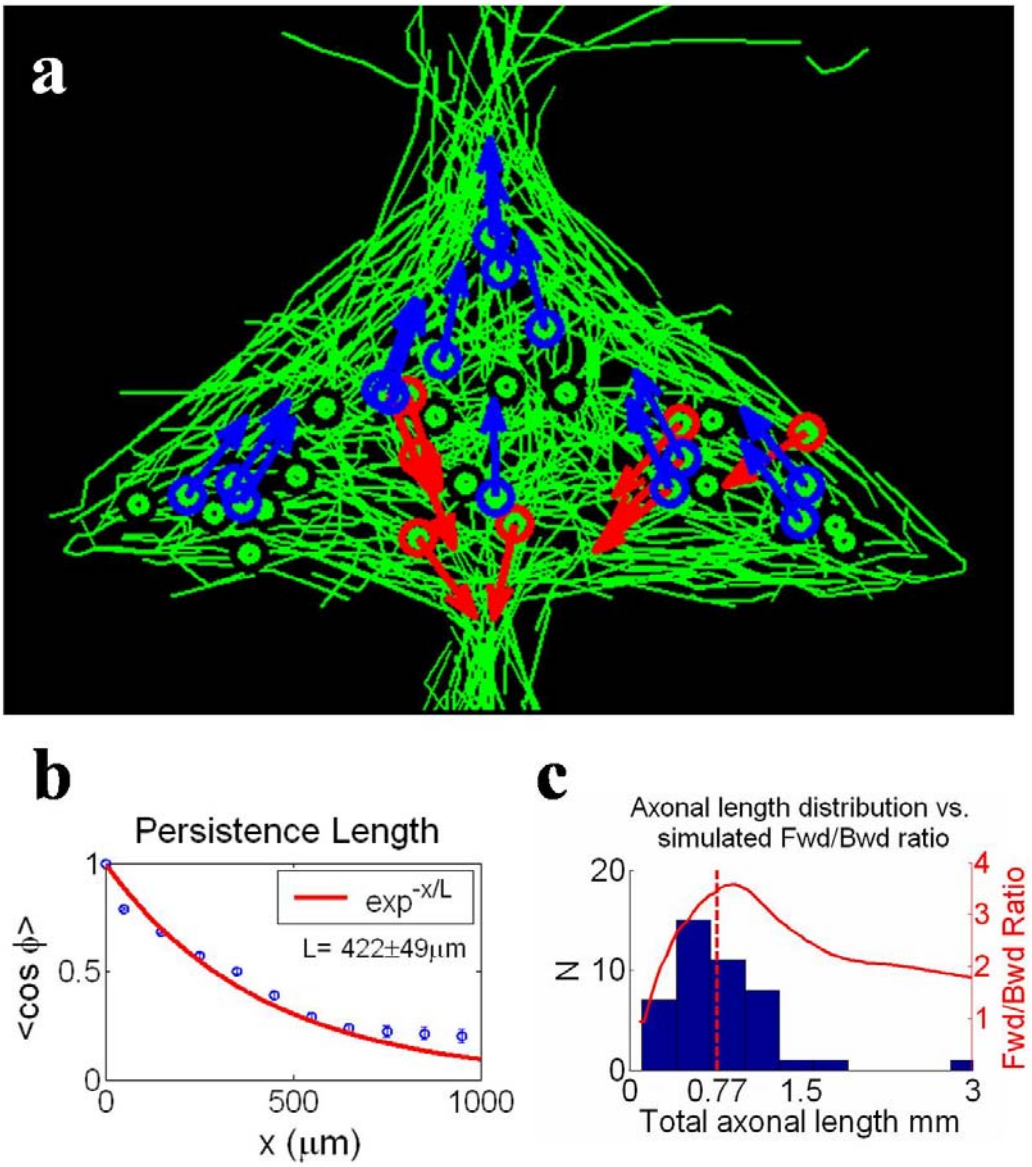

Figure S1: a) Overlaid summary from analysis of 11 GFP images of triangles. Green lines are axon segments that were manually tracked. Circles are coordinates of neuronal cell bodies. Blue circles denote cells with axons that cross forward, which are concentrated on the two sides of the isosceles, while red circles mark cells that cross backwards. The red circles are concentrated along pathways running upwards at an angle of 45° from the apex of the previous triangle, hinting that backward crossing occurs because of axonal growth along pre-existing forward crossing pathways. b) Blue: The mean and standard error of angular difference between all segments that are x μm apart. Red: the persistence length L is the decay length of an exponent that fits the averaged data. c) Blue bars: Experimentally measured histogram of total axonal lengths. Red line: the simulated ratio of forward vs. backward crossings as a function of total axonal length.

It is interesting to compare the behavior of Γ to the experimental axonal length measured in the GFP images. The red line in Figure S1c shows that the maximum ratio of crossings is obtained for axonal lengths of $900\mu m$, close to the experimentally measured mean axonal length of $800\mu m$. The average ratio of forward to backward crossings, weighted by the distribution of axonal length, was $<\Gamma>=3.1$.

D Modeling the response of a Threshold device.

In the spirit of von Neumann's analysis of computational machines or organisms that use unreliable units[5], we introduce a simple description of the Threshold devices. As explained in the text, we connect M Input neurons to one Output neuron. The response of the Output neuron depends both on the number of inputs it receives and on its own response function. The transmission of inputs is where the von Neumann approach is implemented, with each of the inputs having an independent probability η to fail. Initially we use the simplest model available for the response of the Output neuron, the step function (a McCulloch-Pitts neuron[6]) multiplied by a linear function, which assures the proportionality of Output to Input firing rates beyond the threshold. This simple model is solved analytically and is used to demonstrate the relations between η, m_o, M and ε (see section D.1 below).

The second description is the 'Leaky Integrate and Fire' neuron (LIF) with both inhibitory and excitatory inputs, which has enough complexity to give a realistic description so that a numerical comparison to the data can extract the biologically relevant parameters. We have attempted to simplify our models, and claim that our qualitative results are model independent, while extracting the quantitative ones requires some refinement of the model.

In comparing to the experiment, we treat all our devices as modified Threshold devices - the AND gate as two parallel connected Thresholds and the Diode as a combination of a backward and a forward Threshold.

D.1 Variables of our system.

We introduce the following variables and parameters:

α	Normalized number of spikes per Input neuron (variable, between 0 and 1).
α^*	Normalized number of spikes per Output neuron (variable, between 0 and 1).
M	Number of Input neurons that connect to each Output neuron.
ε	The total error rate of the modified Threshold devices.
m_o	Minimum number of excitatory inputs required to make an Output neuron fire (taken from the literature as $m_o=15\pm5$[2, 7-9])
η	The error rate of a single active connection between two neurons.
I	The fraction of Input spikes that are inhibitory (taken as $I=0.3$).
C	Reduction in Input due to asynchrony and incomplete connectivity.
a	Ratio of Output spikes to Input spikes (beyond threshold).

Measured variables. Our experiment provides the fluorescence intensities measured for each burst at the Input and Output regions respectively. The fluorescence is determined by the total number of spikes in the burst. To obtain the normalized average number of spikes per neuron in a burst, amplitudes are calculated from the peaks of the bursts f, normalized per region by its maximum f_{max} and baseline background f_{bgd}:

$$\alpha = \frac{\left(f - f_{bgd}\right)}{\left(f_{\max} - f_{bgd}\right)} \qquad (1).$$

We end up with the two dependent variables (α,α^*) for the Input and Output respectively. The bursts all have a characteristic time scale[10] of *100ms*, so that the number of spikes is equivalent to a firing rate.

For the AND Gate, the Input rate α was taken as the average of the two Input Regions. In the Diode, signals were separated according to either forward or backward propagation.

Measured parameters. The number of Input neurons M that cross the barrier for each modified Threshold was measured as described in section B above. $M = 116, 121, 231$ and 363 for the Threshold, Backwards Diode, AND Gate and Forward Diode respectively.

The total error rate ε of the corresponding modified Thresholds was also measured. The proper function of a logical Threshold device is obtained by finding two thresholds α_t and α_t^* so that if $\alpha>\alpha_t$ then $\alpha^*>\alpha_t^*$ and vice versa. Errors are those bursts that do not fulfill this condition. We found that $\alpha_t^*=0.3, 0.35, 0.2$ and 0.2 for the Threshold component, Backward Diode, AND gate and Forward Diode respectively. Finding α_t entailed an optimization process to minimize the number of errors for every device separately. The total error rate ε per device was calculated by binning and averaging the fraction of erroneous bursts over bins and over samples. The results of this measurements are ε = 6%, 2%, 1.5% and 1% for the Threshold component, Backward Diode, AND gate and Forward Diode respectively. Note that these error rates are related to but different from the error rates (given in Figure 2) of the full AND gate and neuronal Diode taken as logical devices.

D.2 The dependence of Output firing on Input

We are interested in formulating a relation $\alpha^*=Y(\alpha,M)$ between the firing rate of an Output neuron and its inputs. Although some of the neurons in the Output may receive inputs mainly from adjacent neurons in the same Output region, we focus on those neurons that receive sufficient inputs from the Input region to ignite them and assume that their behavior correlates with the rest of the neurons in the Output region. In general, a neuron's activity will depend on the inputs it receives and on its own response function so Y will be the composition of the response and input functions.

The inputs are typically the source of errors, originating in a probability η for failure of signal transmission. This is where we will use von Neumann's combinatorial treatment. The response function of the neuron involves a threshold behavior, with a minimal number m_o of input spikes below which the neuron does not respond at all. Above the threshold value we expect the firing rate of the Output neuron to grow with the number of Input spikes it receives. The probability of the Output neuron itself to fail is negligible[11].

D.3 Calculation of Input

The appropriate scaled variable for the Input is the total number of spikes generated. We define S_{max} as the maximal number of spikes per neuron, averaged over all neurons. Then $X=\alpha S_{max}M$ is the total number of spikes generated at the Input for each event. We will see below (Section D.5.1) that S_{max} is on the order of 4-5 spikes per neuron.

Only a part of the spikes that the Input neurons generate is effective in exciting the Output neuron. The fundamental mechanism for losses that we are interested in is the random failure of transmission of single Input spikes, which we treat as a combinatorial contribution, where different axons fail to transmit a spike at each burst. We have checked that having multiple release sites of vesicles from each synapse gives the same quantitative results within the experimental measurement error.

The existence of inhibitory neurons will decrease the signal as well. The effect of inhibition is accounted by one inhibitory spike canceling one excitatory spike. If $I=0.3$ is

the fraction of inhibition[12] in the Input then an effective fraction of only *1-2I=0.4* of the original number of spikes is available for excitation. Other processes that will reduce the input are the lack of synchrony between neurons and an incomplete connectivity (i.e. not all *M* Input neurons connect to the Output neuron), and we treat these as a constant reduction *C*. If the number of active spikes is denoted X_{in} then the number of spikes available for excitation is $X_{in} \cdot 0.4C$. In the treatment below we embed this correction factor into the modified threshold parameter $m_o^{'}$ (see sub-section D.4.1 below).

The combinatorial loss in transmission is described by a failure of *n* out of the total number of spikes *X* to propagate:

$$X_{in} = X - n \quad (2),$$

with *n* that is distributed binomially with error rate η:

$$P(n) = \binom{X}{n} \eta^n (1-\eta)^{X-n} \xrightarrow[X\to\infty]{} \frac{1}{\sqrt{2\pi}\sigma} e^{-\frac{(n-\mu)^2}{2\sigma^2}} \qquad (3).$$

Note that the probability of a post-synaptic response being generated without a pre-synaptic spike is not taken into account. This is equivalent to failure in transmitting a '1' but not in transmitting a '0'. We approximated *P* for large *X* by a Gaussian distribution with a mean $\mu = X\eta$ and the standard deviation $\sigma^2 = X\eta(1-\eta)$ of the binomial distribution. The approximation is valid since for *X* lower than a hundred there is never a response and *P* is not calculated. We will use this simplified description for the analytic solution of the model in Section D.4.1.

We account for unreliability in inhibition in two ways – in the first model its contribution is assumed to be constant, while in the second we assume a constant fraction *I=0.3* of inhibitory spikes and distinguish between failures of inhibitory and excitatory spikes, denoted n_i and n_e respectively:

$$X_{in} = X + n_i - n_e \qquad (4),$$

We assume an independent probability for n_e failures of excitatory spikes and for n_i failures of inhibitory spikes, each distributed binomially with error rate η:

$$P(n_e, n_i) = \binom{0.7X}{n_e} \eta^{n_e} (1-\eta)^{0.7X-n_e} \binom{0.3X}{n_i} \eta^{n_i} (1-\eta)^{0.3X-n_i} \qquad (5)$$

where we substitute the value of *I=0.3* as the fraction of inhibition and excitation of *X*.

D.4 Calculation of the Output.

The relevant response *Y* of the Output is the number of spikes generated in a single neuron. Since our measured variable α^* is normalized, we must scale it when we want to compare the calculated *Y* to experiment. Since we expect the firing rate of the Output neuron to grow with the number of Input spikes it receives, when we scale the Input by *M* we should also scale the Output proportionally: $Y = M\alpha^*$.

We denote by *y(X,n)* the response to a single realization of the number of failures in excitatory and inhibitory spikes. The total response *Y* will be the weighted average of *y(X,n)* with all possible number of input failures:

$$Y(X) = \sum_n P(n)\, y(X,n) \qquad (6).$$

In the experiment averaging is performed every burst because we measure from multiple neurons, and is then averaged again over different bursts.

In the next two sub-sections two different response functions *y* are considered. In the first sub-section the fraction of inhibitory contribution is non-random and *y=y(X,n)*. In the

second sub-section we take into account the fraction of inhibitory Input spikes and denote by $y(X,n_e,n_i)$ the response to a single realization of the number of failures in excitatory and inhibitory spikes. The total response Y will be also be modified:

$$Y(X)=\sum_{n_e,n_i}\left[P(n_e,n_i)\,y(X,n_e,n_i)\right] \qquad (7)$$

D.4.1 Step Function

We look first at a simple description for the relation of Input and Output that will yield an analytic solution. Probably the simplest description for an errorless neuron is the step function $\Theta(X_{in}-m_o')$ of a McCulloch-Pitts neuron. We assume that the response of an Output neuron has a sharp threshold at m_o'. Below that threshold the neuron does not fire. Once the number of input spikes does exceed m_o' then the neuron begins firing, and the number of spikes that it fires depends linearly on the number of inputs. We use a modified threshold $m_o'=m_o/(0.4C)$ that corrects for the constant reduction of input due to inhibition, asynchrony and incomplete connectivity (see sub-section C.3).

Since we are mainly interested in the transition range we approximate the output response as:

$$y(n)=aX\cdot\Theta\left[(X-n)-m_o'\right] \qquad (8),$$

with a extracted phenomenologically from the data. Plugging this expression and Equation (3) into the sum of equation (6) and transforming the sum into an integral, the number of spikes Y can be evaluated as:

$$\begin{aligned} Y(X) &= \int_0^X P(n)\,y(n)\,dn \\ &= \frac{aX}{\sqrt{2\pi}\cdot\sigma}\int_0^X e^{-\frac{(n-\mu)^2}{2\sigma^2}}\Theta\left[(X-n)-m_o'\right]dn \\ &= \frac{aX}{\sqrt{2\pi}\cdot\sigma}\int_0^{X-m_0'} e^{-\frac{(n-\mu)^2}{2\sigma^2}}\,dn \end{aligned} \qquad (9)$$

This equation holds only if the number of spikes exceeds the threshold $X>m_o'$. To solve the integral we substitute $x=X-m_o'$ and $n'=(n-\mu)/\sigma$:

$$\frac{1}{\sqrt{2\pi}\cdot\sigma}\int_0^{X-m_0'} e^{-\frac{(n-\mu)^2}{2\sigma^2}}\,dn=\frac{1}{\sqrt{2\pi}}\int_{\frac{-\mu}{\sigma}}^{\frac{x-\mu}{\sigma}} e^{-\frac{n'^2}{2}}\,dn'$$

In the relevant range of $X>m_o'$ we use the fact that $\mu/\sigma>>1$ and approximate:

$$\frac{1}{\sqrt{2\pi}}\int_{\frac{-\mu}{\sigma}}^{\frac{x-\mu}{\sigma}} e^{-\frac{n'^2}{2}}\,dn'\approx\frac{1}{\sqrt{2\pi}}\int_{-\infty}^{\frac{x-\mu}{\sigma}} e^{-\frac{n'^2}{2}}\,dn'=\phi\left(\frac{x-\mu}{\sigma}\right)$$

where ϕ is the normal cumulative distribution function:

$$\phi(z)=\frac{1}{\sqrt{2\pi}}\int_{-\infty}^{z} e^{-\frac{u^2}{2}}\,du$$

Plugging back $x=X-m_o'$ and the mean $\mu=X\eta$ and variance $\sigma^2=X\eta(1-\eta)$ of the binomial approximation we get the final analytic approximation for Y:

$$Y(X)=\begin{cases} aX\cdot\phi\left(\dfrac{X-m_o'/(1-\eta)}{\sqrt{X\eta/(1-\eta)}}\right) & X\geq m_o' \\ 0 & X<m_o' \end{cases} \qquad (10)$$

D.4.2 Leaky Integrate and Fire

The simple model above is good for an analytical analysis of the relations between the biological parameters, but does not fit the data well enough for extracting parameter values with satisfying confidence intervals. We have tried to fit data with Non Leaky Integrate and Fire model and found that the LIF model gives best results. However, the confidence intervals for η and m_o' remained high due to their close reciprocal relation (see section D.5). This was resolved by addressing the fact that a significant fraction of the Input spikes is inhibitory. We denote by $y(X,n_e,n_i)$ the response to a single realization of the number of failures in excitatory and inhibitory spikes. The total response Y will be the weighted average of $y(X,n_e,n_i)$ with all possible number of input failures:

The Output neuron is modeled as a 'Leaky Integrate and Fire' neuron[13] with a response function:

$$f=\begin{cases} \dfrac{1}{t_{ref}-\tau\ln\left(1-\frac{m_o'}{X_{in}}\right)} & X_{in}\geq m_o' \\ 0 & o/w \end{cases} \qquad (11)$$

Here t_{ref} is the refractory time of the Output neuron, τ is the membrane time constant and f is the resulting firing rate of the neuron. As before, m_o' includes the effects of inhibition, asynchrony and incomplete connectivity on the threshold value.

For a given Input burst with duration ΔT the number of spikes per neuron is $y=f\cdot\Delta T$ and we get from(11):

$$y(X_{in})=\begin{cases} \dfrac{A}{1-B\ln\left(1-\frac{m_o'}{X_{in}}\right)} & X_{in}\geq m_o' \\ 0 & o/w \end{cases} \qquad (12)$$

where $A=\Delta T/t_{ref}$ is the maximal number of spikes that a neuron can theoretically fire, related to S_{max} but higher than it. The biological parameter $B=\tau/t_{ref}=3$ is taken from the experimental literature[14].
Plugging Equations (5) and (12) into Equation (7) we get:

$$Y(X)=\sum_{n_i=0}^{0.3X}\sum_{n_e=0}^{0.7X}\left[\binom{0.3X}{n_i}\eta^{n_i}(1-\eta)^{0.3X-n_i}\binom{0.7X}{n_e}\eta^{n_e}(1-\eta)^{0.7X-n_e}\frac{A}{1-3\ln\left(1-\frac{m_o'}{X-n_e+n_i}\right)}\right] \qquad (13)$$

D.5 Results and Analysis

D.5.1 Rescaling the data

The scaling of the X and Y variables with the number of neurons M (sub-section D.3) led to the data collapse of all the devices (Figure 4). We now notice that all the modified Thresholds in Figure 4 respond with a very similarly sized jump at the same critical X_t.

Just beyond this transition all Output neurons are assumed to fire exactly once, while at the transition only half of the neurons respond. We normalize and keep the notation Y for the scaled variable so that $Y(X_t)=½$ *spike/neuron*. The full range of Y then occurs at an average maximal number of spikes per neuron $S_{max}=Y_{max}=4.5$ *spikes/neuron*. Since the characteristics of the Input and Output neurons are the same, we can safely assume that the maximal number of spikes in the Y variable is also the scaling for the X variable, $X=\alpha S_{max} M$.

D.5.2 Fitting the data

We fit Equation (13) to the data (Figure 4) and get: $A=\Delta T/t_{ref}=7.3\pm0.8$, $m_o'=148\pm43$ and $\eta=0.64\pm0.08$ with *95%* confidence intervals. The value of η is in good agreement with some of the direct measurements of the probability of a spike to fail[15, 16]. A is the maximal number of spikes that a neuron can theoretically fire. As expected, it is in the scale of S_{max} but higher than it. Substituting the values for the modified threshold $m_o'=m_o/(0.4\cdot C)$ and the number of excitatory input spikes needed for an output neuron to fire $m_o=15\pm5$ [2, 7-9] we get: $C=0.25\pm0.1$. Thus asynchronous spiking and incomplete connectivity reduces the Input by a factor of four.

The LIF model describes well the evolution of the spike rate in a neuron, and gives good agreement with the data in the high X regime, where the Output spiking rate tends toward saturation. It also captures well the low part of the transition region, due to the subtle effect of the inhibitory neurons, which are taken to be independent of the excitatory ones (see Figure 4).

D.5.3 Analytical description of the transition region

Figure 4 in the manuscript exhibits a striking transition from $Y=0$ to $Y=1$ *spike/neuron*, which we can now identify using S_{max} to occur at $X_t=450$. The explanation for this shift in the location of the transition from $m_o'=148$ can be found by rewriting the analytical solution of the step function response (Equation (10)):

$$Y(X) \sim \phi\left(\frac{X - X_t}{\sigma(X)}\right) \qquad (14)$$

$$X_t = \frac{m_o'}{(1-\eta)}$$

$$\sigma = \sqrt{X\eta/(1-\eta)}$$

The transition is shifted from m_o' by a factor of $1/(1-\eta)$ as a result of the errors in transmission.

The reliability of a single Threshold device can now be explained by using Equation (14) and focusing on the transition around X_t. In our experiment we observe that errors in the Output of our devices occur mostly in the transition region (Figure S2). In the von Neumann nomenclature these are the "malfunctions" that are minimized by redundancy[5]. The ratio of the width of the transition to the full X domain is therefore a good estimate for the error rate of the Threshold device. The width of the transition is of the order of σ_t and the extent of the X domain is $S_{max}\cdot M$, so that the error rate ε of a Threshold device is:

$$\varepsilon \approx \frac{\sigma_t}{S_{\max}\cdot M} = \frac{\sqrt{X_t\eta/(1-\eta)}}{S_{\max}\cdot M} \qquad (15)$$

Once the value of $\eta=0.64$ fitted from the LIF model and the corresponding M values are inserted, we get estimates of $\varepsilon=5\%,5\%,3\%$ and 1.5% for the Threshold component, Backward Diode, AND gate and Forward Diode respectively. This compares well with the measured error rates for each of these modified Thresholds, which are $\varepsilon=6\%,2\%,1.5\%$ and 1% respectively (Section D.1).

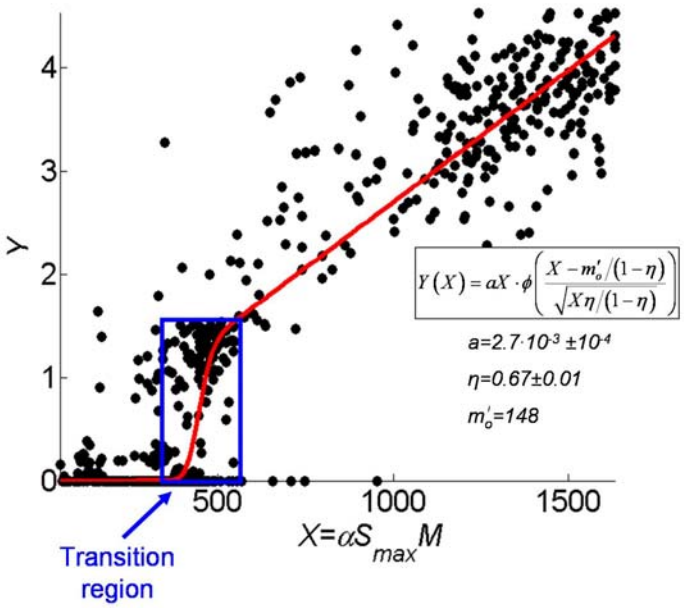

Figure S2: Data points of all (same as the data in Figure 4 in the manuscript) are fitted with the solution of the step function response with $m_o^{'}=148$ fixed at the previously fitted value from the solution of the LIF response function. Blue frame denotes the transition region.

References.

1. Papa, M., Bundman, M. C., Greenberger, V. & Segal, M. Morphological analysis of dendritic spine development in primary cultures of hippocampal neurons. J Neurosci 15, 1-11 (1995).
2. Feinerman, O., Segal, M. & Moses, E. Signal propagation along unidimensional neuronal networks. J Neurophysiol 94, 3406-16 (2005).
3. Rasband, W. S.
4. Thévenaz, P., Ruttimann, U. E. & Unser, M. A pyramid approach to sub-pixel registration based on intensity. IEEE Trans. Image Processing 7, 27-41 (1998).
5. von Neumann, J. in Automata Studies (eds. Shannon, C. & McCarthy, J.) 43-98 (Princeton University Press, 1956).
6. McCulloch, W. S. & Pitts, W. A logical calculus of the ideas immanent in nervous activity. 1943. Bull Math Biol 52, 99-115; discussion 73-97 (1990).
7. Stevens, C. F. Neuronal communication. Cooperativity of unreliable neurons. Curr Biol 4, 268-9 (1994).
8. Breskin, I., Soriano, J., Moses, E. & Tlusty, T. Percolation in living neural networks. Phys Rev Lett 97, 188102 (2006).
9. Thomson, A. M., Deuchars, J. & West, D. C. Large, deep layer pyramid-pyramid single axon EPSPs in slices of rat motor cortex display paired pulse and frequency-dependent depression, mediated presynaptically and self-facilitation, mediated postsynaptically. J Neurophysiol 70, 2354-69 (1993).
10. Jacobi, S. & Moses, E. Variability and corresponding amplitude-velocity relation of activity propagating in one-dimensional neural cultures. J Neurophysiol 97, 3597-606 (2007).
11. Movshon, J. A. Reliability of neuronal responses. Neuron 27, 412-4 (2000).
12. Soriano, J., Rodríguez-Martínez, M., Tlusty, T. & Moses, E. Development of Input Connections in Neural Cultures. Proc Natl Acad Sci U S A in press (2008).
13. Koch, C. Biophysics of computation : information processing in single neurons (Oxford University Press, New York, 1999).
14. Giugliano, M., Darbon, P., Arsiero, M., Luscher, H. R. & Streit, J. Single-neuron discharge properties and network activity in dissociated cultures of neocortex. J Neurophysiol 92, 977-96 (2004).
15. Allen, C. & Stevens, C. F. An evaluation of causes for unreliability of synaptic transmission. Proc Natl Acad Sci U S A 91, 10380-3 (1994).
16. Stevens, C. F. & Wang, Y. Changes in reliability of synaptic function as a mechanism for plasticity. Nature 371, 704-7 (1994).